APPLICABILITY OF FOUR LOCALIZED-CALIBRATION METHODS IN UNDERWATER MOTION ANALYSIS

Young-Hoo Kwon and Steven L. Lindley
Human Performance Laboratory, Ball State University, Muncie, Indiana, USA

Four different localized-calibration methods were developed based on the DLT (direct linear transformation) algorithm in an effort to reduce the error due to refraction in underwater motion analysis. Their applicability in underwater motion analysis was assessed based on a simulated 3D calibration trial with 2 cameras and a hexahedral calibration frame. It was concluded from the analysis of the calibration results that (a) all methods substantially reduced the maximum reconstruction error and demonstrated the potential to minimize object space deformation, (b) localization methods based on overlapped control volumes/areas revealed superior performance than those based on distinct volumes/areas, and (c) the 2D DLT-based localization algorithm provided more accurate object space reconstruction than the 3D DLT-based algorithm.

KEY WORDS: camera calibration, localized calibration, underwater motion analysis, refraction error, object space deformation, reconstruction error

INTRODUCTION: Light refraction in underwater motion analysis introduces pin-cushion-distortion-like errors to the image-plane (digitized) coordinates. Marzan and Karara (1975) proposed an algorithm to correct for this optical distortion. Unfortunately, this algorithm cannot correct the refraction error because, as illustrated in Figure 1, it is impossible to express the refraction error as a function of the image-plane coordinates alone. Although markers M_1 and M_2, shown in Figure 1, both map to point I on the image plane through refraction point R, the magnitudes of the refraction error for the two points differ: $\Delta\mathbf{I}_1$ vs. $\Delta\mathbf{I}_2$. The refraction error included in the image-plane coordinates varies depending on the actual location of the marker.

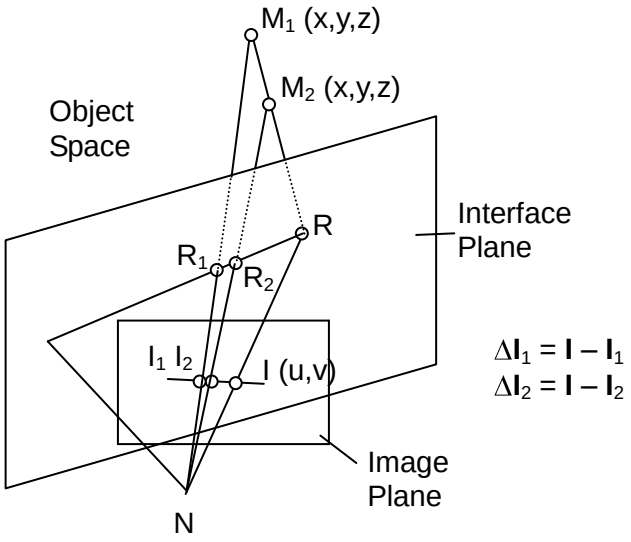

Figure 1 – Errors in the image-plane coordinates due to refraction.

There are two possible approaches to solving the refraction problem in underwater motion analysis: (1) develop new algorithms that can effectively correct the refraction error, and (2) modify the existing algorithms to improve their applicability. For example, Kwon (1999a) took the first approach and reported a new camera calibration algorithm based on hybridization of a geometric refraction-correction procedure and the 2D DLT (direct linear transformation) method. However, this algorithm must be accompanied by an effective optimization procedure to achieve its full potential and a reliable optimization strategy has not yet been reported.

Although the second approach cannot completely eliminate the refraction problem, it is possible to reduce the error by modifying the existing algorithms. The intent of this study was to modify the DLT calibration algorithm, the most commonly used calibration method in underwater motion analysis, to improve its applicability.

The DLT method is based on the collinearity among the node point (point N in Figure 1), the image point (I_1) and the marker (M_1), but light refraction at the water-air (water-glass-air) interface plane distorts this relationship and causes a deformed image: N-I-M_1. During the calibration process, the object-space coordinates of the control points are forced to fit to the deformed image-plane coordinates and the mismatch error must be evenly distributed throughout the control volume. Due to the non-linear pin-cushion-distortion-like nature of refraction, the maximum mismatch error (calibration error) normally occurs at the boundary of the control volume and even larger errors are expected in the case of extrapolation (Kwon, 1999a & 1999b). Distribution of the control points within the control volume can affect the max-to-RMS calibration error ratio, and sectioning of the control volume using multiple cameras can reduce the calibration error (Kwon, 1999b).

Drenk, Hildebrand, Kindler & Kliche (1999) reported an underwater reconstruction method based on two parallel control-point grids (the double-plane method). In each camera view, the marker was projected to the grid planes and the projected 2D coordinates were computed based on the 2D DLT calibration method using the four control points that were closest to the projected marker on each plane. The perspective line connecting the two projected points was defined from each camera view. The intersection of the perspective lines obtained from multiple camera views yielded the 3D coordinates of the marker.

The idea of sectioning the control volume using multiple cameras, suggested by Kwon (1999b) as a method to reduce the refraction error, can be further exploited. One may intentionally section the control volume regardless of the number of camera views and strategically localize camera calibration and object space reconstruction to reduce the error due to refraction. The purpose of this study was to develop a systematic and flexible localization strategy and to assess the applicability of the localized-calibration methods in 3D underwater motion analysis.

METHODS: A total of 4 localized-calibration methods (2 algorithms x 2 localization strategies) were developed in this study based on the DLT algorithm. Methods O/3 and NO/3 were based on the 3D DLT algorithm while methods O/2 and NO/2 used the double-plane 2D DLT algorithm, the generalized version of the calibration technique developed by Drenk et al. (1999). The typical DLT algorithm was modified to accommodate the localized-calibration and reconstruction procedures.

Localization of the calibration and reconstruction was achieved mainly through grouping of the control points, with each group defining a unique control volume (O/3 & NO/3) or area (O/2 & NO/2). Two different grouping (localization) strategies were used in this process: overlapping (O) and non-overlapping (NO). The O methods (O/3 & O/2) were based on a group of overlapping control volumes/areas while the NO methods (NO/3 & NO/2) were based on a set of distinct, non-overlapping control volumes/areas.

The calibration/reconstruction program was designed to allow the user to easily define the control groups. For a given marker position, the program identifies the closest control point group to the marker and performs the calibration/reconstruction based on this group — localization. In the double-plane method, the perspective line connecting the two projected points on the planes was identified in each camera view for the subsequent 3D reconstruction using the least-square method.

Figure 2 shows the calibration frame (28 control points) and the control volumes/areas used in this study. The Y-axis of the calibration frame was aligned in the swimming direction. All 5 volumes (100 cm x 100 cm x 100 cm, HWD, each) shown in Figure 2b were used in method O/3 while only volumes 1, 3 and 5 were used in method NO/3. Twelve control points were used to define each control volume. Similarly, all 10 areas shown in Figure 2c (100 cm x 100 cm, HW, each) were used in method O/2 while only areas 1-1, 1-3, 1-5, 2-1, 2-3 and 2-5 were used in method NO/2. Six control points were used to define each control area.

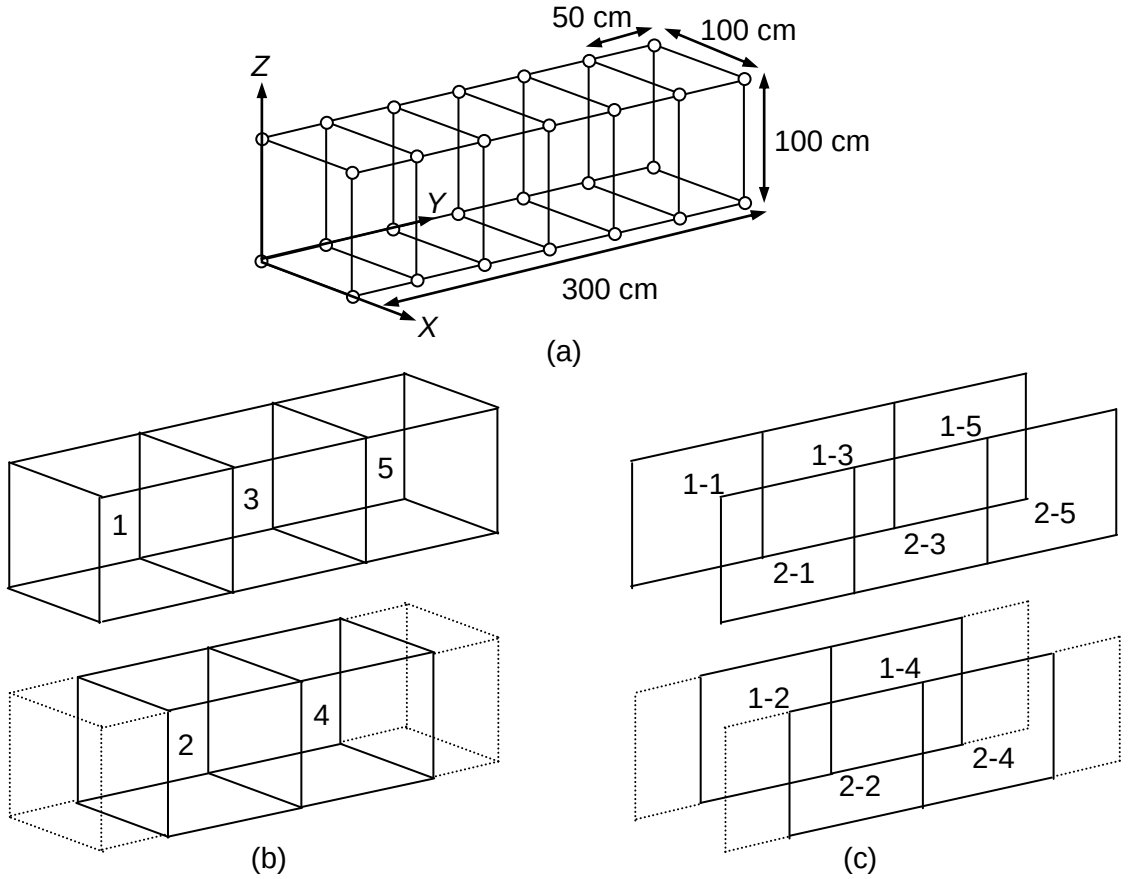

Figure 2 – Calibration frame (a) and the control volumes (b) & areas (c) formed by the control point groups.

The reconstruction errors were computed from a simulated calibration trial rather than an actual experiment. Figure 3 shows the simulated camera setup used in this study. The calibration frame was positioned 5 cm below the water surface while the cameras were set at 55 cm below (z = 50 cm). The refraction model described by Kwon (1999a) was used in generating the refracted image-plane coordinates. The calibration algorithms and the refraction model were incorporated into the Kwon3D motion analysis software to generate the simulated image-plane coordinates and to perform the subsequent calibration/reconstruction. The RMS and maximum reconstruction errors were computed.

RESULTS AND DISCUSSION:

Reconstruction Errors. Table 1 summarizes the reconstruction results of the localized-calibration methods. Also included in the table are the reconstruction results that were obtained using the conventional 3D DLT method for comparison. All localized-calibration methods scored substantially smaller calibration errors than the 3D DLT method. The RMS errors of methods O/3, NO/3, O/2 and NO/2 were equivalent to 37.4 %, 32.2 %, 41.4 %, and 36.2 % of the error that occurred with the 3D DLT method, respectively. The maximum calibration errors were 24.7 % (O/3 & NO/3), and 23.7 % (O/2 & NO/2) of that of the 3D DLT method. The maximum errors of the localized-calibration methods showed smaller relative values to the 3D DLT method than the RMS errors indicating the localization produced positive effects on the maximum reconstruction error. Methods with overlapping (O/3 & O/2) scored slightly larger RMS value than their NO counterparts while the 3D DLT-based methods (O/3 & NO/3) showed smaller RMS errors than their 2D DLT-based counterparts. However, it is important to note that the RMS reconstruction error is generally not the best index of an accurate calibration/reconstruction (Kwon, 1999b).

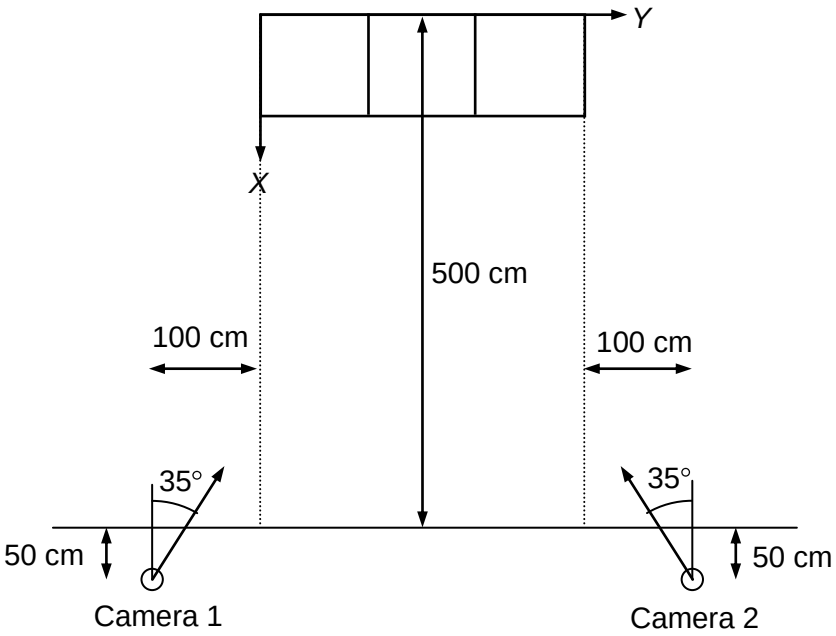

Figure 3 – Simulated camera setup.

Table 1 **Reconstruction Results (Unit: cm)**

	RMS Error	Max. Error	Max-to-RMS Ratio
3D DLT	1.74	3.93	225.9 %
O/3	0.65	0.97	149.2 %
NO/3	0.56	0.97	173.2 %
O/2	0.72	0.93	129.2 %
NO/2	0.63	0.93	147.6 %

The localized-calibration methods also resulted in smaller max-to-RMS reconstruction error ratios than the conventional 3D DLT method (Table 1). This implies that the localized-calibration approach clearly had positive impact on the extrapolation errors. The max-to-RMS error is a useful indicator of the severity of the extrapolation errors because the maximum error normally occurs at the boundary of the control volume/area (Kwon, 1999a & 1999b).

Object Space Deformation. Although the reconstruction errors (RMS & maximum) are commonly used as the measure of the overall accuracy of the camera calibration/reconstruction, they do not reflect the details of object space deformation within the control volume. The non-linear nature of the refraction error increases the chance of object space deformation. One way to investigate the severity of the object space deformation is to track the 3D coordinates of the known markers continuously moving along the prescribed paths. To accomplish this, 4 straight lines of motion passing through the control volume were identified (Figure 4). The Y-coordinate changed from -100 cm to 400 cm with increments of 2 cm. Because the cameras were set at z = 50 cm, only the upper half of the control volume was examined.

As summarized in Figure 5, the reconstructed length (L) of each 2-cm interval fluctuated as the Y position changed. The fluctuation in the reconstructed interval length indicates the severity of the object space deformation along the Y-axis. The 3D DLT method showed continuous length-position curves with trends of underestimation errors in the middle of the control volume and large overestimation errors near the boundary and outside. Although the localized-calibration methods generally demonstrated substantially less object space deformation (area under the length-position curve about L = 2 cm) throughout the control

volume and in the extrapolation region, discontinuity in the object space (spikes in the length-position curves) was observed. These spikes were caused by the switching of the control volumes/areas, as predicted by Kwon (1999b). Methods O/2 and NO/2 were characterized by multiple consecutive spikes due to the switching of the control areas in both planes (Figure 2). One can expect discontinuity in the object space in any calibration method dealing with a set of control volumes, including the panning methods (Yanai, Hay & Gerot, 1996). It is interesting to note that lines 1 and 3 in method NO/3 (Figure 5c) lack the spikes at the discontinuity region because the analysis program could not generate the reconstructed 3D coordinates. The program used an iterative approach to obtain a stable set of coordinates and to find the closest control volume/area to the current marker position. Repeated switching, back and forth, between two adjacent control volumes prevented the coordinates from converging. This incident provided an important implication: intentional use of missing points at the discontinuity region as a mean to reduce the severity of the discontinuity.

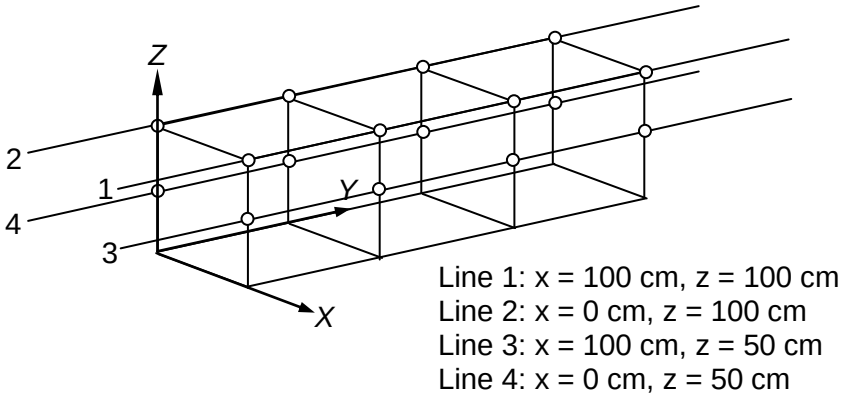

Figure 4 – Locations of the continuous lines of motion used in assessing the object space deformation. The Y-coordinate ranged from -100 cm to 400 cm.

Methods O/3 and O/2 revealed spikes of smaller amplitudes than methods NO/3 and NO/2. This is because overlapping of the control volumes assures switching to occur before the marker reaches the boundary of the current control volume/area, thus, decreasing the amount of space deformation. This was the main idea behind the localization strategy with overlapped control volumes/areas and this comparison maintains that the localization strategy is effective. On the other hand, methods O/2 and NO/2 revealed spikes of smaller amplitudes than their 3D DLT-based counterparts. The 2D DLT-based double-plane algorithm also demonstrated more accurate length estimation throughout the entire Y-coordinate range. One may speculate some possible explanations: (1) a control area can be fit to the refracted image more accurately than a control volume, and (2) the X-coordinates of the planes are already known so that the refraction errors affect the coordinates of the projected points in a limited fashion. Further investigation may be necessary. Method O/2 was identified as the best localized-calibration method among the 4 methods used.

The discontinuity problem must be treated properly to maximize the applicability of the localized-calibration approach. Although data filtering will ease the discontinuity problem to some extent, one may take additional measures such as (1) developing a strategy to temporarily tag the marker as missing at the discontinuity region so that the program later generates interpolated coordinates, and (2) using more complex control point grouping and overlapping schemes with smaller control volumes. The first approach involves modification of current software while the second requires greater initiative from the investigator. Although increasing the camera-to-interface distance and/or the interface-to-calibration-frame distance will certainly reduce discontinuity (Kwon, 1999b), it is not regarded as an ultimate solution.

A more sound approach to tackle the discontinuity problem is to develop a panning method that is based on a continuous control volume/area. The panning method can be placed under the umbrella of localization since it meets the basic requirements of the localized-calibration

method: sectioning of the control volume/area. Use of a continuous control volume in the panning method can eliminate switching of the control volumes/areas.

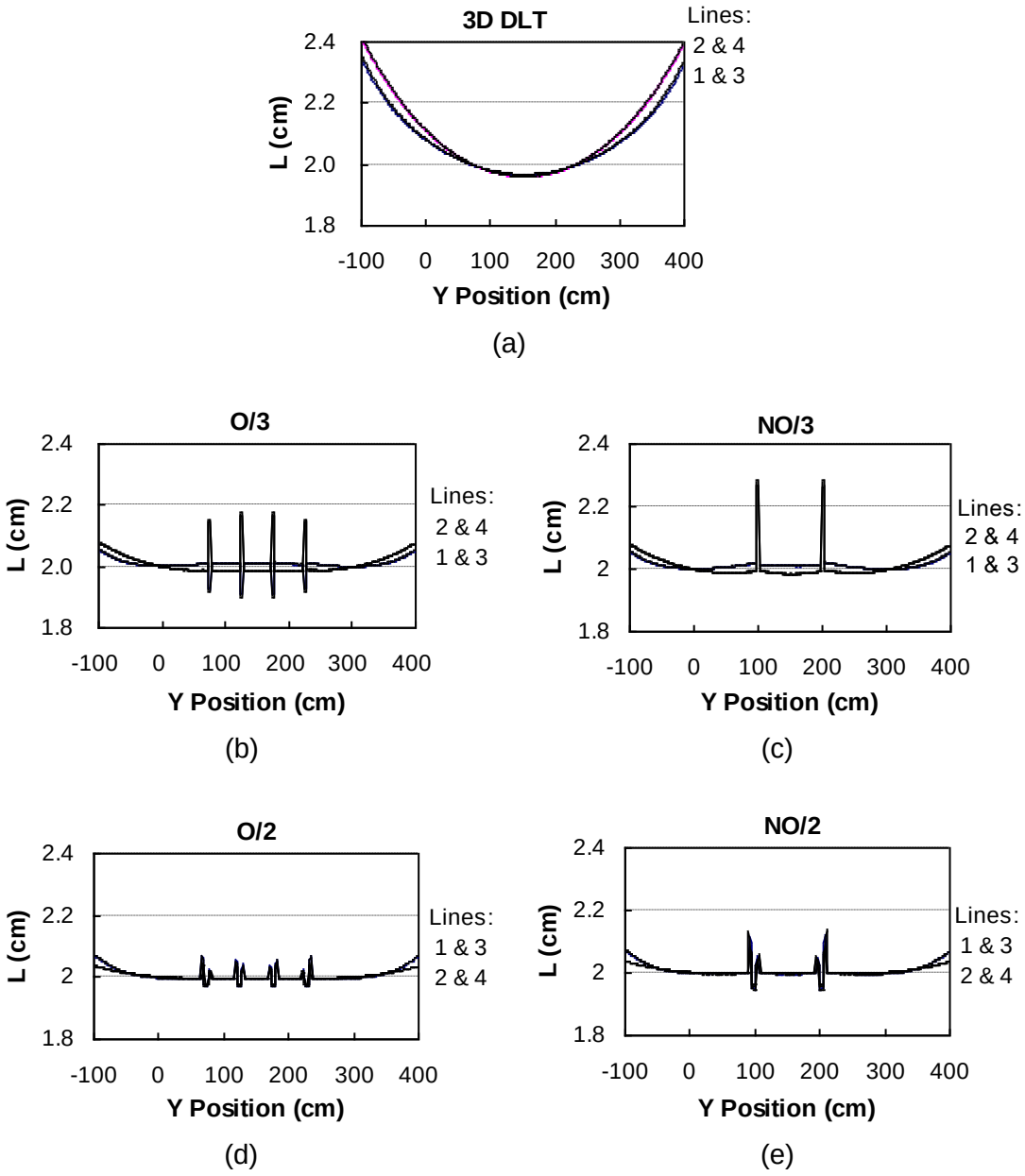

Figure 5 – Object space deformation in the 3D DLT method (a) and in the localized calibration methods: O3 (b), NO/3 (c), O/2 (d), and NO/2 (e). The reconstructed length of the 2-cm interval (L) was plotted for the Y position.

Discontinuity in the Object Space at the Water Surface. In underwater motion analysis it is often essential to combine the position data obtained from the underwater camera views with those obtained from the above-water views. For example, Cappaert et al. (1995) computed the location of the shoulder both from the underwater views and from the above-water views, respectively, and forced them to coincide with each other by translating the coordinates obtained from the underwater views. This strategy appears to be the result of a large discrepancy in the shoulder position at the water surface. Since the discontinuity in the object space at the water surface can affect the overall accuracy of the analysis, the object space discontinuity at the water surface level was assessed based on two known straight lines of motion located above the calibration frame at the water surface (x = 0 & 100 cm, z = 105 cm).

See Figure 2 for the details of the coordinate system setup. The Y-coordinate varied from -100 cm to 400 cm with increments of 2 cm. The 3D coordinates reconstructed from the underwater views were compared with the actual coordinates for the computation of the mismatch error.

Table 2 Maximum Position Mismatch Error at the Water Surface (Unit: cm)

Method	Control Region	Extrapolation Region
3D DLT	4.23	15.93
O/3 & NO/3	1.13	8.19
O/2 & NO/2	0.74	9.91

As shown in Table 2, the localized-calibration methods scored substantially smaller maximum position mismatch errors than the 3D DLT method at the water surface in both the control region and the extrapolation region. The mismatch errors in the control region were 26.7 % (O/3 & NO/3) and 17.5 % (O/2 & NO/2) of the error that occurred with the 3D DLT method, while those in the extrapolation region were equivalent to 50.8 % and 62.2 % of the 3D DLT method, respectively. When compared with the errors in the control region, the mismatch errors in the extrapolation region revealed larger values relative to the 3D DLT method. This is a contradiction to our general findings. (Table 1 & Figure 5). Further analysis revealed that the mismatch error of the localized calibration methods in the extrapolation region was almost exclusively from the X-coordinate, which appeared to be related to the camera setup (70° between the camera axes) used in this study. Since the swimmer's shoulders and arms generally do not reach the lateral boundary of the control volume when they leave the water, the actual mismatch error should be somewhat smaller than those reported in Table 2. However, one must pay close attention to the position mismatch error at the water surface in the extrapolation region.

CONCLUSION: It was concluded from the analysis of the calibration results that (a) the DLT-based localized-calibration methods substantially reduced the reconstruction error, especially the maximum error, (b) the localized-calibration methods revealed the potential to substantially reduce the object space deformation throughout the control volume, (c) the localized-calibration methods based on a set of mutually overlapping control volumes/areas revealed superior performance than those based on distinct, non-overlapping volumes/areas, and (d) the 2D DLT-based localized-calibration methods provided more accurate object space reconstructions than the 3D DLT-based methods.

The localized-calibration methods can be especially useful in a poor experimental setup with short camera-to-interface distance (waterproof camera housing) and/or short interface-to-control-volume distance (flume) since these settings cause a substantial increase in the magnitude of the error due to refraction (Kwon, 1999b).

REFERENCES:

Cappaert, J.M., Pease, D.L., & Troup, J.P. (1995). Three-dimensional analysis of the men's 100-m freestyle during the 1992 Olympic Games. *Journal of Applied Biomechanics*, **11**, 103-112.

Drenk, V., Hildebrand, F., Kindler, M., & Kliche, D. (1999). A 3D video technique for analysis of swimming in a flume. In R.H. Sanders & B.J. Gibson (Eds.), *Scientific Proceedings of the XVII International Symposium on Biomechanics in Sports* (pp. 361-364). Perth, Australia: Edith Cowan University.

Kwon, Y.-H. (1999a). A camera calibration algorithm for the underwater motion analysis. In R.H. Sanders & B.J. Gibson (Eds.), *Scientific Proceedings of the XVII International Symposium on Biomechanics in Sports* (pp. 257-260). Perth, Australia: Edith Cowan University.

Kwon, Y.H. (1999b). Object plane deformation due to refraction in two-dimensional underwater motion analysis. *Journal of Applied Biomechanics,* **15**, 396-403.

Marzan, G.T. & Karara, H.M. (1975). A computer program for direct linear transformation

solution of the collinearity condition, and some applications of it. In *Proceedings of the Symposium on Close-Range Photogrammetric Systems* (pp. 420-476). Falls Church, VA: American Society of Photogrammetry.
Yanai, T., Hay, J.G., and Gerot, J.T. (1996). Three-dimensional videography of swimming with panning periscopes. *Journal of Biomechanics*, **29**, 673-678.